NeuroImage 78 (2013) 372–384

Contents lists available at SciVerse ScienceDirect

NeuroImage

journal homepage: www.elsevier.com/locate/ynimg

fMRI hemodynamics accurately reflects neuronal timing in the human brain measured by MEG

Fa-Hsuan Lin [a,b,*], Thomas Witzel [c,1], Tommi Raij [c,1], Jyrki Ahveninen [c,1], Kevin Wen-Kai Tsai [a], Yin-Hua Chu [a], Wei-Tang Chang [a,c], Aapo Nummenmaa [b,c], Jonathan R. Polimeni [c], Wen-Jui Kuo [d], Jen-Chuen Hsieh [d,e], Bruce R. Rosen [c], John W. Belliveau [c]

[a] Institute of Biomedical Engineering, National Taiwan University, Taipei, Taiwan
[b] Department of Biomedical Engineering and Computational Science, Aalto University School of Science, Espoo, Finland
[c] Harvard Medical School, Athinoula A. Martinos Center for Biomedical Imaging, Department of Radiology, Massachusetts General Hospital, Charlestown, MA, USA
[d] Institute of Neuroscience, National Yang-Ming University, Taipei, Taiwan
[e] Institute of Brain Science, National Yang-Ming University, Taipei, Taiwan

ARTICLE INFO

Article history:
Accepted 5 April 2013
Available online 13 April 2013

Keywords:
Neurovascular coupling
Hemodynamics
Neuronal timing
Inverse imaging
Latency
BOLD

ABSTRACT

Neuronal activation sequence information is essential for understanding brain functions. Extracting such timing information from blood oxygenation level dependent (BOLD) fMRI is confounded by interregional neurovascular differences and poorly understood relations between BOLD and electrophysiological response delays. Here, we recorded whole-head BOLD fMRI at 100 ms resolution and magnetoencephalography (MEG) during a visuomotor reaction-time task. Both methods detected the same activation sequence across five regions, from visual towards motor cortices, with linearly correlated interregional BOLD and MEG response delays. The smallest significant interregional BOLD delay was 100 ms; all delays ≥400 ms were significant. Switching the order of external events reversed the sequence of BOLD activations, indicating that interregional neurovascular differences did not confound the results. This may open new avenues for using fMRI to follow rapid activation sequences in the brain.

Introduction

Discerning the interregional order of neuronal activations is indispensable for understanding how the brain works. Unfortunately, following activation sequences throughout the brain is complicated by the fact that different imaging technologies offer compromises between spatial and temporal resolution. Functional MRI (fMRI) of the human brain (Belliveau et al., 1991) with blood oxygenation level dependent (BOLD) contrast (Kwong et al., 1992; Ogawa et al., 1992) has millimeter spatial resolution (Menon and Kim, 1999), but can only detect slow vascular responses that lag the underlying neuronal events by seconds (Logothetis et al., 2001). Moreover, BOLD signals may show strong voxel-to-voxel latency variability at individual level data (Lee et al., 1995). fMRI has thus been believed to be excellent for spatial localization but unsuitable for studying fast, dynamic spread of neuronal activations across brain areas. On the other hand, temporally precise electrophysiological methods such as magneto- and electroencephalography (MEG/EEG) that record neuronal activity directly suffer from uncertainties in source localization and are mainly sensitive to generators in superficial brain areas (Hämäläinen et al., 1993).

Owing to high spatial resolution of fMRI and excellent temporal resolution of MEG/EEG, integration of data across modalities might allow spatiotemporally accurate brain imaging (for a recent review, see Rosa et al., 2010). Physiological support to such attempts comes from studies indicating tight coupling between neuronal and vascular events in the somatosensory system of rodents (Devor et al., 2003) and human visual system (Sharon et al., 2007). Thus, fMRI, a vascular marker of neuronal events, could be used as a physiological constraint to reduce the spatial ambiguity in the source localization inverse problem of MEG/EEG. For example, the equivalent current dipole (ECD) fitting method in MEG/EEG source localization can be informed by fMRI (Ahlfors et al., 1999; George et al., 1995; Vanni et al., 2004). The statistical maps derived from fMRI data can also be used as a spatial prior for the distributed source reconstruction (Dale et al., 2000; Liu et al., 1998, 2002). A further study using simulations demonstrated the advantage of combined fMRI and EEG for a higher efficiency of cortical current density estimation at different SNR with the presence of both fMRI visible and fMRI invisible sources (Babiloni et al., 2003). It has also been shown that integrating fMRI and MEG can improve the localization of cortical sources of MEG oscillatory activity (Lin et al., 2004).

* Corresponding author at: Institute of Biomedical Engineering, National Taiwan University, 1, Sec. 4, Roosevelt Road, Taipei, 106, Taiwan.
E-mail address: fhlin@ntu.edu.tw (F.-H. Lin).
[1] These authors contributed equally to this work.

1053-8119/$ – see front matter © 2013 Elsevier Inc. All rights reserved.
http://dx.doi.org/10.1016/j.neuroimage.2013.04.017

Yet, some aspects of BOLD signals may surprisingly accurately reflect neuronal timing. For example, animal studies have shown that sequential neuronal activations can modulate the fMRI signal amplitude at a time scale of tens of milliseconds (Ogawa et al., 2000). Furthermore, event-related fMRI (Dale and Buckner, 1997; Rosen et al., 1998) studies have suggested that the durations of the BOLD response in motor planning areas correlate with behavioral reaction times (Menon et al., 1998; Richter et al., 2000), that onsets and durations of BOLD responses can be used to infer the functional roles of different language-related brain areas (Bellgowan et al., 2003), and that relative delays between visual hemifield stimuli correlate with interhemispheric BOLD latency differences (Huettel and McCarthy, 2000; Menon et al., 1998). Timing differences across brain areas have also been reported in previous event-related BOLD chronometry studies (Kim and Ogawa, 2002; Rosen et al., 1998 for reviews), but only when employing tasks with long (~1–10 s) reaction times that inflate the delays between sensory and motor areas (Formisano et al., 2002; Miezin et al., 2000; Richter et al., 1997, 2000; Sigman et al., 2007) and/or by strongly limiting spatial coverage to increase sampling frequency (Menon et al., 1998; Richter et al., 2000). Acknowledging that interregional vasculature differences (both across neighboring and more distant voxels) may confound BOLD timing information (Lee et al., 1995; Miezin et al., 2000), it has not yet been confirmed whether such results reflect genuine neuronal timing sequences, or rather, interregional neurovascular differences. Moreover, while some studies have compared generator mechanisms between BOLD signals and local field potentials (Logothetis et al., 2001), there are no prior reports that examine the interregional timing between BOLD and magneto- or electroencephalographic (MEG/EEG) responses. The origins of small (about 100–600 ms) interregional delays in BOLD recordings, thus, have remained a topic of speculation.

Here, we hypothesize that by using a sufficiently high whole-head sampling frequency, group-level fMRI hemodynamic responses (HDR) can reveal even very rapid neuronal activation sequences throughout the brain. To test this hypothesis, we utilize inverse imaging (InI) BOLD fMRI, which samples the entire brain at 100-ms temporal resolution (TR = 100 ms) while offering about 5-mm cortical spatial accuracy (Lin et al., 2008, 2010). First, to examine the putative confounds that may arise from interregional differences in vasculature, we measured BOLD timing differences when the order of external events was reversed (visual → motor *vs.* motor → visual) and found that the magnitude of such confounds is, at group level, quite small. Second, supported by both magnetoencephalographic (MEG) and behavioral reaction time (RT) data, we demonstrate that BOLD fMRI can provide reasonable temporal estimates of neuronal activation sequences.

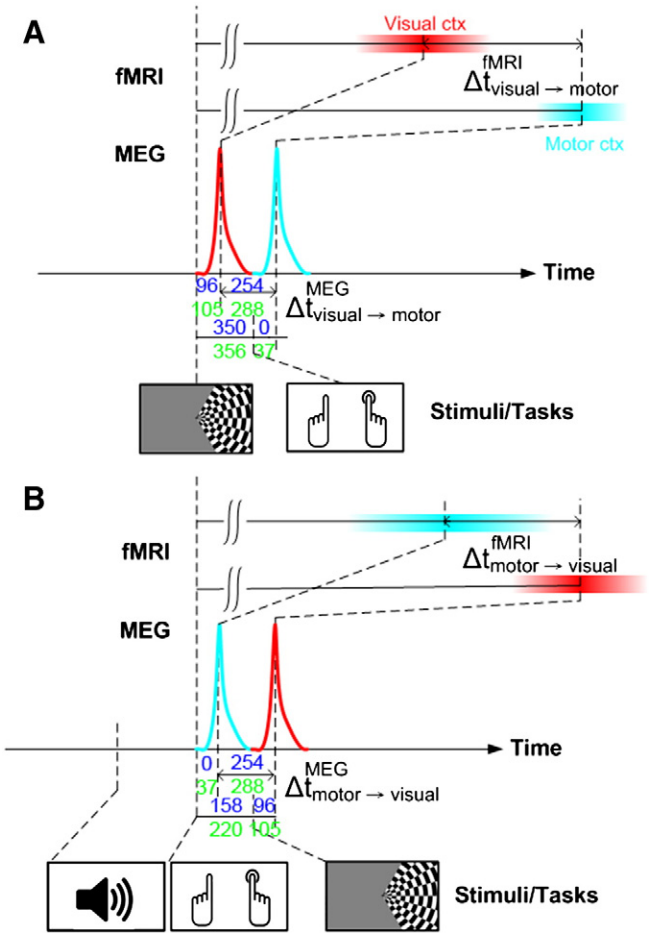

Fig. 1. Stimuli and tasks. (A) In the main visuomotor experiment, subjects were presented with visual hemifield stimuli and asked to push a button with the ipsilateral hand as quickly as possible, thus eliciting visual and motor cortex activations in the contralateral cerebral hemisphere. Half of the trials were on the right and half on the left hemifield. The corresponding neuronal timings were recorded with MEG, and the hemodynamic timings with fMRI. $\Delta t^{MEG}_{visual \rightarrow motor}$ represents the neuronal delay from the visual to the motor cortex and $\Delta t^{fMRI}_{visual \rightarrow motor}$ the BOLD delay from the visual to the motor cortex. BOLD latencies are delayed with respect to the neuronal latencies due to neurovascular coupling. (B) In the control experiment the stimulus-task order was flipped (motor response before visual stimulus, with onset of trials cued by an auditory tone). The delay between the button press and presentation of the visual stimulus was set such that the expected neuronal delay from the motor to the visual cortex $\Delta t^{MEG}_{motor \rightarrow visual}$ would be equal to $\Delta t^{MEG}_{visual \rightarrow motor}$ observed in the main experiment. $\Delta t^{fMRI}_{motor \rightarrow visual}$ represents the BOLD delay from the motor to the visual cortex. Actual values for all timing indices are labeled in the figure (blue texts: right hand/hemifield; green texts: left hand/hemifield).

Materials and methods

Subjects, stimuli, and tasks

All subjects were right-handed healthy adults. Written informed consent in accord with the National Taiwan University Hospital and National Yang Ming University ethical committees was obtained prior to participation. The study encompassed three experiments: a main fMRI experiment (n = 21, 6 females, age 22–30 years), a control fMRI experiment (n = 12, 8 females, age 21–28 years), and an MEG experiment (n = 8, 4 females, age 21–30 years).

Visual stimuli in all experiments were left or right hemifield reversing (8 Hz) checkerboard stimuli presented in random order. Stimulus duration was 500 ms. The stimuli subtended 4.3° of visual angle and contained 24 evenly distributed radial wedges and eight concentric rings of equal width. The stimuli were presented using Psychtoolbox (Brainard, 1997; Pelli, 1997).

In the main fMRI visual → motor experiment (Fig. 1A), timing of each visual stimulus was randomized with a uniform distribution of interstimulus intervals (ISIs) varying from 4 to 16 s (mean 10 s). The subjects were instructed to press the button with the hand ipsilateral to the visual stimulus as soon as possible. Thus, the experiment included two conditions: right visual hemifield — right hand (R) and left visual hemifield — left hand (L). Twenty-four trials were presented during four 240 s runs, resulting in a total of 96 trials per subject.

The control fMRI motor → visual experiment (Fig. 1B) was designed to reverse the order of neuronal activations in the visual and somatomotor cortices. Binaural auditory cues (1 kHz and 4 kHz sinusoidal waveforms with 200 ms duration) were presented randomly with ISI varying from 4 to 16 s (mean 10 s). Subjects were asked to respond with the left or right hand pushbutton after hearing a 200-ms tone pip (1 kHz for left and 4 kHz for right hand response). Subsequently, a visual checkerboard in the hemifield ipsilateral to the button press was presented. The latency between the button press and the onset of visual stimulation was 158 ms for the right and 220 ms for the left hand/hemifield. These latencies, based on the MEG experiments described below, were chosen such that the absolute neuronal timing

difference between visual and motor cortices would be the same in the control experiment as in the main experiment (Fig. 1). Each run included 24 trials using left hand to respond and 24 trials using right hand to respond. Four 240 s runs were collected. To calculate reaction time, only trials with RTs within the mean ± 1.5 SD were included in further analyses.

Structural MRI acquisition

All MRI data were measured on a 3 T scanner (Tim Trio, Siemens Medical, Erlangen, Germany) with a 32-channel head coil array. Parameters used to acquire structural MRI were: repetition time/echo time/inversion time [TR/TE/TI] = 2530/3.49/1100 ms, flip angle = 7°, partition thickness = 1.33 mm, image matrix = 256 × 256, 128 partitions, field-of-view = 21 cm × 21 cm. The location of the gray–white matter boundary for each participant was estimated with an automatic segmentation algorithm to yield a triangulated mesh model with approximately 340,000 vertices for both hemispheres (Dale et al., 1999; Fischl et al., 1999a, 2001). This cortical surface model was then used to facilitate mapping of the structural image from native anatomical space to a standard cortical surface space (Dale et al., 1999; Fischl et al., 1999a). Across-subjects averaging was done by morphing individual data through a spherical surface (Fischl et al., 1999b).

Inverse imaging acquisition and reconstruction

The InI *reference scan* (a full gradient encoding scan needed to collect the spatial information in the coil array for subsequent image reconstruction) was collected using a 3D segmented (one shot per partition) echo-planar imaging (EPI) readout, after exciting one thick coronal slab covering the entire brain (FOV 256 mm × 256 mm × 256 mm; 64 × 64 × 64 image matrix) with the flip angle set to the gray matter Ernst angle of 30° (considering that the T_1 of the gray matter is 1 s at 3 T). Partition phase encoding was used to obtain the spatial information along the anterior–posterior axis. The EPI readout had frequency encoding along the superior–inferior and phase encoding along the left–right axis. We used TR = 100 ms, TE = 30 ms, bandwidth = 2604 Hz/pixel and a 12.8 s total acquisition time for the reference scan, allowing the coverage of the whole-brain volume with 64 partitions and two repetitions.

The InI *functional scans* used the same volume prescription, TR, TE, flip angle, and bandwidth as the InI reference scan. The principal difference was that, to achieve high temporal resolution, partition phase encoding was removed so that the full volume was excited, and the spins were spatially encoded by a single-slice EPI trajectory, resulting in a coronal *X*/*Z* projection image with spatially collapsed projection along the anterior–posterior direction. The *k*-space InI reconstruction algorithm (Lin et al., 2010) was then used to estimate the spatial information along the anterior–posterior axis. In each run, we collected 2400 measurements after discarding the first 32 measurements in order to reach the longitudinal magnetization equilibrium. A total of 4 runs of data were acquired from each participant.

InI reconstruction

Analysis of the InI data across all RF coil array channels and across all time points consists of two separate linear processes occurring in both spatial and temporal domains (Lin et al., 2008, 2010). First, we processed the data in the time domain in order to calculate the coefficients of the hemodynamic response basis function within each voxel of the projection image in each coil channel separately. Specifically, we used Finite-Impulse-Response (FIR) basis function (Burock and Dale, 2000) and General Linear Model (GLM) to allow a high degree of freedom in characterizing dynamic responses to avoid bias in estimating the shape of the hemodynamic responses. Confounds of low frequency oscillations characterized by sinusoidals (<0.01 Hz), linear drift, run-specific DC shift, and the global mean of each instantaneous measurements were also included in the GLM. Second, we reconstructed the 3D distribution of the HDR basis function coefficients in the spatial domain using *k*-space InI reconstruction (K-InI) (Lin et al., 2010), which offers approximately 5 mm spatial resolution at the cortex when InI data are sampled using a 32-channel head coil array at 3 T. One practical benefit of this order of reconstructing the InI data is that the temporal reconstruction can first reduce the dataset size eight fold (2400 samples per run to 300 samples, the number of our FIR basis function over the duration of our chosen HDR). K-InI reconstruction is a generalization of parallel MRI in *k*-space (Lin et al., 2010). The missing k-space data were linearly interpolated from other *k*-space locations from the ensemble of all channels of the coil array. The interpolation coefficients were estimated from the InI reference scan. The K-InI method produces a coil-by-coil image reconstruction. The final volumetric reconstruction was calculated as the sum-of-squares combination of the images from all reconstructed channels in the array. In fMRI, we are interested in estimating the statistically significant activity spatiotemporally. The noise levels in the reconstructed images were estimated from the baseline data in the 4-second window occurring immediately before the onset of the first sensory stimulus (visual stimuli in the main experiment and auditory stimuli in the control experiment), after K-InI reconstruction. Using these noise estimates, dynamic statistical parametric maps (dSPMs) were derived as the time-point by time-point ratio between the K-InI reconstruction values and the baseline noise estimates. dSPMs are *t* distributed under the null hypothesis of no hemodynamic response (Dale et al., 2000).

To transform the functional results into individual cortical surface space, the spatial registration between InI reference and native space anatomical data was calculated using the FSL toolbox (http://www.fmrib.ox.ac.uk/fsl), estimating a 12-parameter affine transformation between the volumetric InI reference and the MPRAGE anatomical space. The resulting spatial transformation was subsequently applied to each time point of the reconstructed K-InI hemodynamic estimates to spatially transform the signal estimates to a standard cortical surface space (Dale et al., 1999). Before spatial transformation, reconstructed K-InI data were spatially smoothed with a 10 mm full-width-half-maximum (FWHM) 3D Gaussian kernel. This smoothing kernel was chosen to be 2.5 times the native image resolution (4 mm in our reference scan). Inter-subject averaging was done by morphing each individual's data through a spherical coordinate system (Dale et al., 1999; Fischl et al., 1999a).

Hemodynamic time course processing

All ROIs were determined by the spatial distribution of the temporally averaged *t* statistics greater than 10.0 (Bonferroni corrected p-value < 0.05) at 3–8 s after the first sensory stimulus onset (visual stimuli in the main experiment and auditory stimuli in the control experiment). The same criteria were used for both the main and the control experiments for ROI selection. This interval was chosen *a priori* to capture the BOLD response positive maximum. Time courses were extracted and averaged within ROIs for each subject separately.

For visualization, group-average time courses were linearly scaled such that their maximum was 1. To quantify timing of the responses, three timing indices were derived after normalizing the peak amplitudes across ROIs: (i) *Onset* was picked at the first time point exceeding 2 standard deviations of the noise level estimated from the pre-stimulus baseline; (ii) *Time-to-half* (*TTH*) was found at 50% of the peak value; and (iii) *Time-to-peak* (*TTP*) was recorded at the maximum of the response. Based on physiological grounds, we hypothesized *a priori* that of these three indices, *TTH* would offer the most accurate interregional temporal estimates. *Onset*, by definition, rises

less above noise level than *TTH* and *TTP*, and is therefore more subject to random effects of noise.

To evaluate the variability of the fMRI timing indices within a ROI in group-average data, we first randomly selected a specific proportion (10–90%) of voxels within each ROI and then calculated the corresponding timing index. This process was repeated 100 times, and we calculated the corresponding mean ± SEM values within each ROI.

A separate analysis was done to evaluate the variability of the fMRI timing indices as a function of the subject in the group-average data. Data from either 1, 2, 4, 8, 12, 16, or 21 subjects were randomly chosen and then the corresponding timing index was calculated. This procedure was repeated 100 times. We particularly calculated the difference between visual and somatomotor cortices to investigate if these two areas show statistically significant timing difference.

MEG stimuli

In the MEG experiment, subjects were presented with the exact same stimuli and tasks as in the main fMRI experiment (Fig. 1A).

MEG acquisition and preprocessing

306-Channel MEG (VectorView, Elekta-Neuromag Oy, Helsinki, Finland) was recorded in a magnetically shielded room (Ahonen et al., 1993; Cohen et al., 2002; Hämäläinen et al., 1993). MEG signals were band-pass filtered at 0.03–200 Hz and digitized at 600 Hz. Electro-oculogram (EOG) was recorded to monitor eye-movement artifacts. All epochs exceeding 150 μV or 3000 fT/cm at any EOG or MEG channel, respectively, were automatically discarded from the offline averages.

MEG source analysis

The co-registration between MEG and MRI coordinates was done by manually registering three fiducial points (left ear, right ear, nasion) between the MEG and structural MRI data. MEG source locations were calculated using Minimum-Norm Estimates (MNEs) from combined anatomical MRI and MEG data (Dale et al., 2000; Liu et al., 1998, 2002). MEG source space was constructed on cortical surfaces with ~7000 vertices per hemisphere. A gain matrix **A**, describing the ensemble of MEG sensor measurements with a unit current dipole on each source vertex, was calculated using a realistic boundary element model (BEM) (Hämäläinen and Sarvas, 1989) based on the high spatial resolution MRI data. Noise covariance matrix **C** was estimated from baseline data without visual stimulation. These two matrices were used to calculate the inverse operator $\mathbf{W} = \mathbf{A}^{\mathrm{T}}(\mathbf{A}\mathbf{A}^{\mathrm{T}} + \mathbf{C})^{-1}$. The MEG data $\mathbf{y}(t)$ at time t were then multiplied by **W** to yield the estimated source activity in the cortical surface: $\mathbf{x}(t) = \mathbf{W}\,\mathbf{y}(t)$. Noise normalization estimates were calculated as $\mathbf{dSPM}(t) = \mathbf{x}(t) / \sqrt{(\mathrm{diag}(\mathbf{WCW}^{\mathrm{T}})}$, where diag is the operator extracting the diagonal vector from a square matrix to display the activations using *F*-statistic (Dale et al., 2000).

The MEG ROI selection was guided with the fMRI ROIs as follows: 1) The fMRI cortical surface ROIs were transformed to the MEG cortical surface source space. 2) For each fMRI ROI, its center on the cortical surface was identified. 3) The MEG source waveform peak latency (the time when the MEG signal was maximal) for the center location was measured. 3) The MEG ROI was delineated by thresholding the group-average dSPM values at the peak latency with a value of 4.5 (*F*-statistic, Bonferroni corrected $p < 0.01$). Due to the complexity of the MEG source waveform, we only picked the time-to-peak (*TTP*) to characterize MEG timing.

Oscillatory MEG analysis

Trials of MEG raw data of 3.3 s duration with 0.8 s pre-stimulus baseline were used to calculate the time-frequency representations (TFRs). Specifically, trial *i*'s spectrotemporally localized complex-value TFR $\mathbf{s}_i(w,t)$ was calculated by convolving the MEG data $\mathbf{y}(t)$ with a Morlet wavelet with 7 cycles $\mathbf{s}_i(w,t) = \int \mathbf{y}(t-\tau) e^{-jw\tau} e^{-\tau^2/2\sigma^2} d\tau, \sigma = 7 \times 2\pi/w$ (Lachaux et al., 1999). Such a choice of σ gave an effective temporal resolution about 3.5 cycles (depending on the frequency *w*). The frequency of the Morlet wavelet *w* ranged between 5 Hz and 36 Hz to cover the alpha, beta, and the sensorimotor mu-rhythm (Hari et al., 1997; Salmelin and Hari, 1994). MEG source power $\mathbf{p}(w,t)$ was estimated by averaging the power of the product between the inverse operator **W** and each trial's TFR $\mathbf{s}_i(w,t)$ across n_{trial} trials: $\mathbf{p}(w,t) = \sum_{i=1}^{n_{trial}} |\mathbf{W}\mathbf{s}_i(w,t)|^2$. $\mathbf{p}(w,t)$ was calculated for all source locations and then averaged within the ROI. Then the baseline value of $\mathbf{p}(w,t)$ was subtracted and the standard deviation of the baseline-corrected $\mathbf{p}(w,t)$ was computed. Lastly, the normalized power was calculated as the ratio between instantaneous baseline-corrected $\mathbf{p}(w,t)$ and the standard deviation of the baseline-corrected $\mathbf{p}(w,t)$ (Lin et al., 2004).

Temporal spectral evolution (TSE) (Salmelin and Hari, 1994) MEG analysis reflects total neuronal activations (both in- and out-of-phase components) and is therefore expected to correlate with BOLD better than evoked MEG responses. TSE for each ROI was calculated as integrating $\mathbf{p}(w,t)$ over 5–36 Hz (Fig. 5B). This frequency range included the characteristic frequency bands for all ROIs. To emphasize event-related synchronization (ERS)/event-related de-synchronization (ERD) components that should best correlate with BOLD signals, we constructed a Gamma-shaped window function $w(t) = \mathrm{Gamma}((t - t_{\mathrm{ERS}}) / \lambda, a, b)$, where parameters ($\lambda = 22$, $a = 2$, $b = 8$) were chosen such that the function captured the ERS/ERD but excluded the rebound, and the peak of this function was set at the ERS peak latency t_{ERS} for each ROI (Fig. 5C). The TSE time courses were then multiplied with the $w(t)$ function for each ROI individually, and the 50% level of the cumulative oscillatory power (Fig. 5D) within the first 2 s after the visual stimulus onset was used as the oscillatory timing index (*OTI*).

Statistical testing of interregional time courses for InI and MEG

Variances of the timing indices were estimated using bootstrapping (Chernick, 2007). Specifically, for the fMRI main experiment, 21 time courses were sampled with replacement from the pool of 21 subjects for each ROI independently. Similarly, for the fMRI control experiment, the analysis was performed using 12 time courses from the pool of 12 subjects, and for the MEG experiment, using 8 time courses from the pool of 8 subjects, for each ROI independently. These time courses were then averaged and fitted by the procedure described above to generate three timing indices. The procedure was repeated 100 times. The variability of the timing indices was then calculated from the standard deviation of the corresponding timing indices across the 100 bootstrap iterations.

Results

In the main experiment (Fig. 1A) subjects ($n = 21$) were presented with 500-ms visual hemifield checkerboard stimuli at random intervals and asked to respond with their left index finger to stimuli appearing in the left hemifield (RT 350 ± 48 ms, mean ± SEM) and with their right index finger to stimuli in the right hemifield (RT 356 ± 45 ms). The average hit rate was 99.1%. The strongest fMRI activations were observed in the hemisphere contralateral to the visual stimulus/motor response (Fig. 2A); thus, results for the left hemifield stimuli are reported in the right hemisphere and for the right hemifield stimuli in the left hemisphere.

In our first timing analysis, we compared only the group-average visual (V) and motor (M) ROI latencies (for spatial extent of ROIs and BOLD time courses, see Figs. 2A and C; for corresponding numerical results see Tables 1 and 2). As illustrated by the data points above

the 45° line, V was activated earlier than M cortex (Fig. 3A). Variance of the group average timing indices was estimated using bootstrapping (Chernick, 2007) with 100 iterations. False-positive rates were non-parametrically quantified by the percentage of data points below this 45° line. All three indices were earlier in the visual than in the motor cortex in the left hemisphere ($p = 0.01$, 0.01, and 0.03 for *Onset*, *TTH* and *TTP*, respectively). In the right hemisphere, *TTH* suggested that the hemodynamic response at the visual cortex preceded that at the motor cortex ($p < 0.01$; *Onset* and *TTP* with $p = 0.12$ and 0.40 respectively) hemisphere. Among the three timing indices, *TTH* showed the smallest variance (Table 1). Therefore, analogous to several previous studies (Descamps et al., 2012; Liu et al., 2005; Waugh et al.,

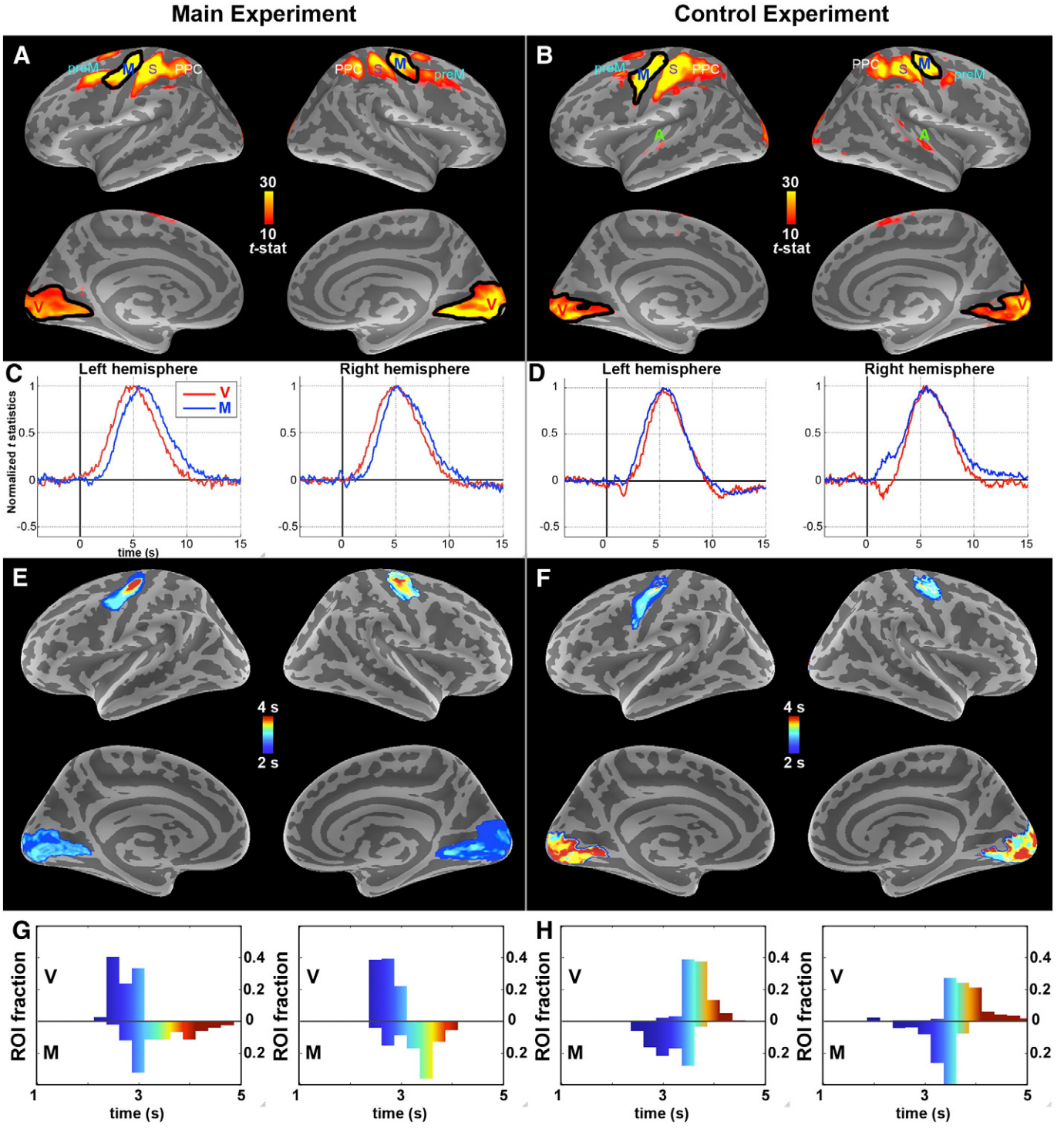

Fig. 2. fMRI activations collapsed at 3–8 s and ROI selections; ROI-specific BOLD time courses; within-ROI BOLD *TTH* distributions. (A) During the main (visuomotor) experiment, both visual (V) and motor (M) cortices were activated. The black outlines indicate the ROIs thresholded from these statistical images. PPC: posterior parietal cortex; S: somatosensory cortex; preM: premotor cortex. (B) During the control (motor–visual) task, V and M cortices were activated. Again, the black outlines indicate the ROIs; these were over 80% overlapping with the main experiment ROIs in panel A. PPC: posterior parietal cortex; S: somatosensory cortex; preM: premotor cortex. (C–D) The corresponding ROI-specific BOLD responses (peak amplitudes normalized across ROIs, group level). The order of activations clearly follows the order of external events (stimuli and task). The signal-to-noise ratio across all ROIs was 29. (E–F) Spatial distribution of latencies (*TTH*) within the visual and motor ROIs. Variability within ROIs was much smaller than delays across ROIs, suggesting that voxel-to-voxel variability did not confound the results. (G–H) Histograms of latencies (*TTH*) within the visual and motor ROIs.

Table 1
BOLD latencies for *Onset*, time-to-half (*TTH*), and time-to-peak (*TTP*) timing index in the five ROIs (mean ± SEM). PPC: posterior parietal cortex.

ROI	Onset (ms)	TTH (ms)	TTP (ms)
A. Left hemisphere			
Visual	1000 ± 180	2800 ± 190	5000 ± 390
PPC	1800 ± 390	2900 ± 170	4700 ± 500
Premotor	1300 ± 410	2900 ± 280	5500 ± 670
Somatosensory	1400 ± 310	3200 ± 130	5400 ± 270
Motor	2200 ± 450	3400 ± 180	5500 ± 340
B. Right hemisphere			
Visual	1000 ± 230	2800 ± 170	5000 ± 280
PPC	1500 ± 510	3100 ± 220	5200 ± 350
Premotor	2200 ± 450	3300 ± 240	4600 ± 290
Somatosensory	2200 ± 460	3300 ± 160	5200 ± 280
Motor	2200 ± 500	3400 ± 130	5200 ± 210

2008; Weilke et al., 2001) and consistent with our prediction that *TTH* may offer more robust estimates than *Onset* and *TTP*, *TTH* was considered the most reliable measure of HDR latency (results for *Onset* and *TTP* are, however, reported as well; see Tables 1 and 2).

BOLD *TTH* of the visual cortex led that of the motor cortex by 600 ms in both the left and the right hemisphere ($p < 0.01$ independently for both; Fig. 3C blue lines). This suggested that BOLD signals could differentiate the timing between visual (input) and motor (output) cortices even though the spread of neuronal activation and reaction times was very fast.

Because the order of activations measured with BOLD could be influenced by interregional differences in brain vasculature, we conducted a control experiment designed to reverse the order of activations (Fig. 1B). Subjects ($n = 12$) pushed a button with the left or right hand after hearing 200-ms tone pips (1 kHz for the left and 4 kHz for the right hand response). RTs were 570 ± 50 ms for the left and 550 ± 50 ms for the right hand. After the button press, a 500-ms visual hemifield checkerboard appeared ipsilateral to the motor response. The delay between the button press and the visual stimulus was 158 ms for the right and 220 ms for the left hemifield; these values were chosen such that the neuronal delay derived from the MEG experiment (see below) across the visual and motor cortices would be equal between the main experiment (Fig. 1A $\Delta t^{MEG}_{visual \rightarrow motor}$) and the control experiment (Fig. 1B $\Delta t^{MEG}_{motor \rightarrow visual}$). Source analysis revealed expected BOLD activations in the motor and visual cortices (Fig. 2B; the time courses of the HDR at the motor and visual cortices are shown in Fig. 2D). Additional early activations related to the auditory stimuli were observed in the auditory cortices (not shown). The visual and motor cortex ROIs in the control experiment overlapped with those in the main experiment by more than 80% (Figs. 2A–B). The activations occurred 600 ms earlier ($p < 0.01$) in the motor than in the visual cortex in the left hemisphere and 500 ms earlier ($p < 0.01$) in the right hemisphere (Figs. 3B, C red lines). This double dissociation excludes the possibility that the order of activations in the main experiment was caused by interregional differences in vasculature. It is useful to note that the interregional delays were fully reversed (0 ms asymmetry) across the main and control experiments in the left hemisphere and almost entirely reversed (100 ms asymmetry) in the right hemisphere ($p = 0.79$, *n.s.*). Therefore, the influence of interregional vasculature differences was small (0–100 ms, statistically non-significant) compared with the interregional delays (500–600 ms). Finally, the possibility that ROI selection and/or voxel-to-voxel variability might have biased the timing results was excluded with auxiliary analyses, where we studied the spatial distribution of *TTH* timing and parametrically changed the ROI size to see how interregional timing changes (Figs. 2E–H). We found that when the proportion of selected voxels was gradually increased from 10% to 90%, the mean values approached the full-ROI values and the SEMs decreased. However, already at 10% proportion the values were relatively close to the full ROI values, and the changes from 10% to 90% were much smaller than the observed interregional ROI delays. Further, even at 10% proportion all latency differences between the visual and motor cortices were significant ($p \leq 0.01$) for both hemispheres and both the main and control experiments individually. Therefore, voxel-to-voxel variability was too small to significantly confound the interregional delay results.

A previous study has suggested high inter-individual vascular variability as a factor that may bias BOLD latency estimates (Aguirre et al., 1998). Thus, in an additional control analysis, we studied how many subjects are needed to reduce the vasculature confounds and

Table 2
BOLD delays between ROIs in the main visuomotor experiment. A significant value implies sequential spread of activity from one ROI to another (* $p \leq 0.05$; p values were corrected for multiple comparisons by controlling the false discovery rate). The smallest statistically significant difference was 100 ms, but most 100 ms delays were statistically non-significant. At the 200–300 ms range, about 50% of delays were significant, and at ≥400 ms all delays were significant.

Left hemisphere Onset

Latency difference [ms]		FROM Visual	PPC	Premotor	Somatosensory	Motor
TO	Visual					
	PPC	800 *				
	Premotor	300	–500			
	Somatosensory	400 *	–400	100		
	Motor	1200 *	400	900	800	

Right hemisphere Onset

Latency difference [ms]		FROM Visual	PPC	Premotor	Somatosensory	Motor
TO	Visual					
	PPC	500				
	Premotor	1200 *	700			
	Somatosensory	1200 *	700	0		
	Motor	1200 *	700 *	0	0	

Left hemisphere TTH

Latency difference [ms]		FROM Visual	PPC	Premotor	Somatosensory	Motor
TO	Visual					
	PPC	100				
	Premotor	100	0			
	Somatosensory	400 *	300 *	300		
	Motor	600 *	500 *	500 *	200 *	

Right hemisphere TTH

Latency difference [ms]		FROM Visual	PPC	Premotor	Somatosensory	Motor
TO	Visual					
	PPC	300				
	Premotor	500 *	200			
	Somatosensory	500 *	200	0		
	Motor	600 *	300 *	100	100 *	

Left hemisphere TTP

Latency difference [ms]		FROM Visual	PPC	Premotor	Somatosensory	Motor
TO	Visual					
	PPC	–300				
	Premotor	500	800			
	Somatosensory	400	700	–100		
	Motor	500	800	0	100	

Right hemisphere TTP

Latency difference [ms]		FROM Visual	PPC	Premotor	Somatosensory	Motor
TO	Visual					
	PPC	200				
	Premotor	–400	–600			
	Somatosensory	200	0	600		
	Motor	200	0	600	0	

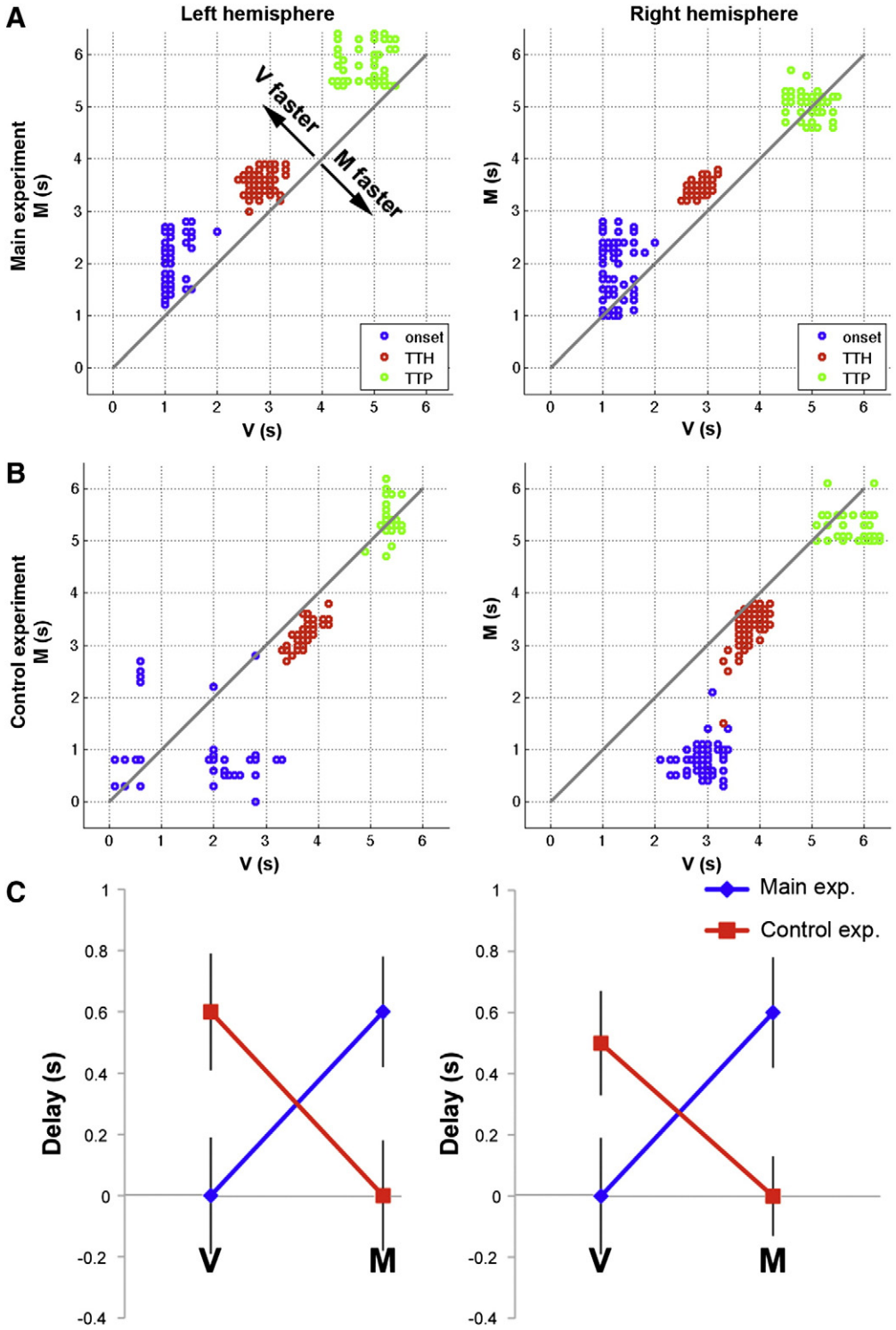

Fig. 3. Hemodynamic response timing in the visual and motor cortices in the main and the control experiments. (A) In the main experiment, the visual cortex (V) was activated before the motor (M) cortex (values above the 45° line) in both hemispheres for all three timing indices. The dots display the 100 bootstrap iterations. (B) In the control experiment, where the order of the stimulus and motor response was reversed (button press followed by visual stimulus), the order of BOLD activations was also reversed such that the motor cortex was activated before the visual cortex (values below the 45° line). (C) BOLD *TTH* delays between the visual and motor cortices in the main (blue) and control (red) experiments (SEM error bars). This result indicates that BOLD timing closely follows the order of external events and is only weakly confounded by interregional vascular differences.

to obtain reliable inter-regional latency estimates. The results suggest that at least eight subjects were required to conclude significant ($p < 0.05$) temporal difference between the visual and motor cortices.

In our subsequent, spatially more detailed analysis of the main fMRI experiment, we observed a sequence of activations across five ROIs, first in the visual cortex, and thereafter propagating to the posterior parietal (PPC), premotor, somatosensory, and finally, the motor cortex (Tables 1 and 2). Locations of the PPC, premotor, and somatosensory cortices are shown in Figs. 2A and B. The results were highly similar across hemispheres. The *TTH* differences between

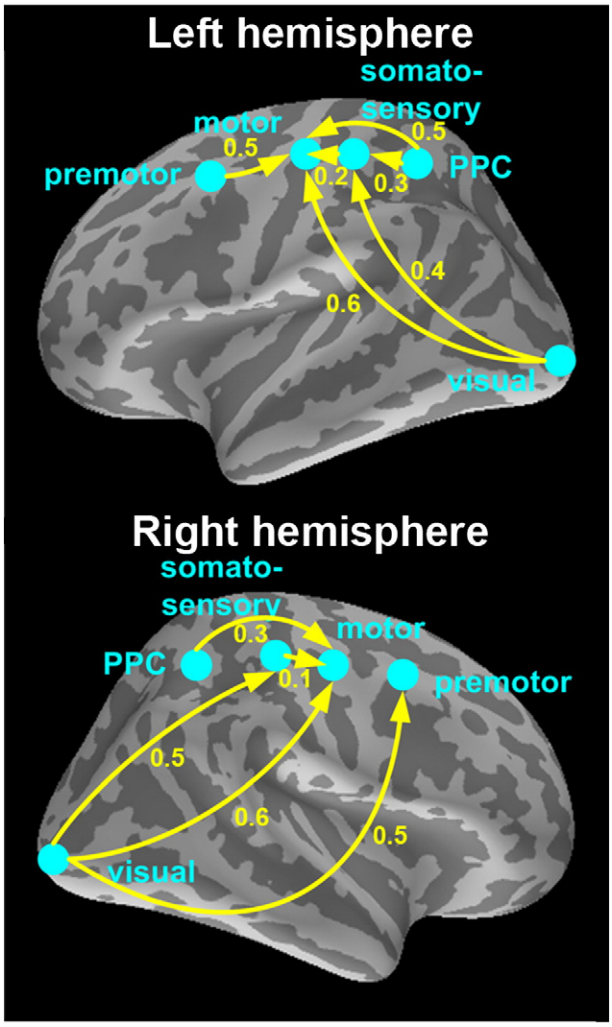

Fig. 4. Latency differences between all five ROIs and direction of activation propagation. BOLD responses were found in the visual, posterior parietal (PPC), premotor, somatosensory, and motor cortices; their approximate locations are illustrated on lateral views of the inflated cortex (for actual source locations see Figs. 2A–B). Yellow arrows indicate direction of activation propagation. Solid arrows indicate $p \leq 0.05$ for the latency difference between any two areas; numerical values show the differences in seconds.

ROIs (arrows in Fig. 4) could be used to infer directional information flow. Across hemispheres, *TTH* difference between motor cortices was non-significant ($p = 0.31$), consistent with that the RTs were similar between the left and right hand stimuli/responses.

To investigate if the above fMRI main experiment hemodynamic timing differences reflect truly neuronal delays we conducted an MEG experiment ($n = 8$) using an identical design. The button press reaction times were 378 ± 71 ms and 340 ± 90 ms for the left and right hemifield visual stimuli, respectively. Source analyses of evoked MEG responses showed group-level activations similar to fMRI results: the distance between the center-of-mass of the ROI determined by fMRI and MEG data independently was less than 10 mm. The evoked MEG response analysis revealed a progression of neuronal activations from the visual to PPC/premotor, somatosensory, and finally, the motor cortices in both hemispheres (Table 3 and Figs. 5A–B). However, the evoked MEG responses only reflect neuronal activations that are both time- and phase locked to the stimuli (out-of-phase components are canceled during averaging across trials), and may thus not optimally correspond to BOLD responses that are driven by all time-locked neuronal events regardless of their phase (Niessing et al., 2005). Therefore, we conducted an additional induced response (temporal spectral evolution or TSE) (Salmelin and Hari, 1994) analysis where phase cancelations do not occur. As expected, the ROI-specific TSE time courses (Figs. 5C–D) showed an early ERS followed by ERD, and finally a strong rebound. Since BOLD generator areas are better correlated with electrophysiological ERS/ERD than with rebound (Brookes et al., 2005; Formaggio et al., 2008; Muthukumaraswamy and Singh, 2008), we constructed an induced response *oscillatory timing index* (*OTI*) that only reflects ERS/ERD timing (Figs. 5E–F). The corresponding latencies (Table 4) revealed a mainly similar order of activations as for the evoked MEG responses, but the interregional delays were much more similar between BOLD and *OTI* (derived from induced responses) than between BOLD and evoked responses.

To quantify the timing relationship between hemodynamic and neuronal measurements, we performed linear regression analyses between the BOLD and MEG results. The evoked MEG responses showed a statistically significant ($p = 0.011$ for the left and 0.008 for the right hemisphere) linear relationship between BOLD *TTH* and MEG *TTP* (Fig. 6A; for regression on BOLD *Onset* and *TTP* with MEG *TTP*, see Figs. 6C and D). The results were similar across hemispheres (for *Y* intercepts, *t*-test: $p = 0.81$, difference *n.s.*; for slopes, *t*-test: $p = 0.33$, difference *n.s.*). Interestingly, interregional delays appeared to be over two times longer in fMRI than in MEG (slope = 2.08 for the left and 1.86 for the right hemisphere).

The MEG delays derived from induced responses (*OTI* in Fig. 6B) were also linearly correlated with BOLD *TTH* delays ($p = 0.04$ for the left and 0.07 for the right hemisphere). Importantly, the slope was, clearly, not statistically different from 1 (*t*-test $p = 0.85$ for the left and 0.96 for the right hemisphere), suggesting that the interregional delays for induced MEG and BOLD signals were similar.

Discussion

The present results suggest that fMRI could resolve even relatively small neuronally driven temporal delays between cortical areas. The results were highly replicable across hemispheres for the two conditions stimulating different visual hemifields. The BOLD response in the visual cortex preceded that in the motor cortex, with intermediate delays in the PPC, premotor, and somatosensory cortices; furthermore, the interregional hemodynamic delays were linearly correlated with the neuronal delays (Fig. 6). Taken together, these results demonstrate that BOLD fMRI may detect the same temporal order of activations as neuronal MEG measurements even during rapid propagation of activity and fast reaction times (~350 ms).

Importantly, the order of BOLD activations followed the timing of external events, as when we switched the order of the visual stimulus and the motor output, the BOLD timings also reversed accordingly (Fig. 3). This double dissociation cannot be explained by either different shapes of regional HDRs or regional vascular differences. In earlier studies it has always remained a possibility that BOLD latency differences

Table 3
MEG evoked response latencies (*TTP*) and MEG induced response oscillatory timing index (*OTI*) latencies for all five ROIs (mean ± SEM).

	Latency [ms]	Visual	PPC	Premotor	Somatosensory	Motor
MEG evoked response latencies	Left hemisphere	96 ± 29	169 ± 7	171 ± 8	349 ± 24	350 ± 75
	Right hemisphere	105 ± 19	187 ± 23	319 ± 63	371 ± 48	393 ± 66
MEG induced response latencies	Left hemisphere	480 ± 56	592 ± 68	640 ± 155	647 ± 62	1037 ± 214
	Right hemisphere	432 ± 93	635 ± 58	726 ± 196	608 ± 37	971 ± 201

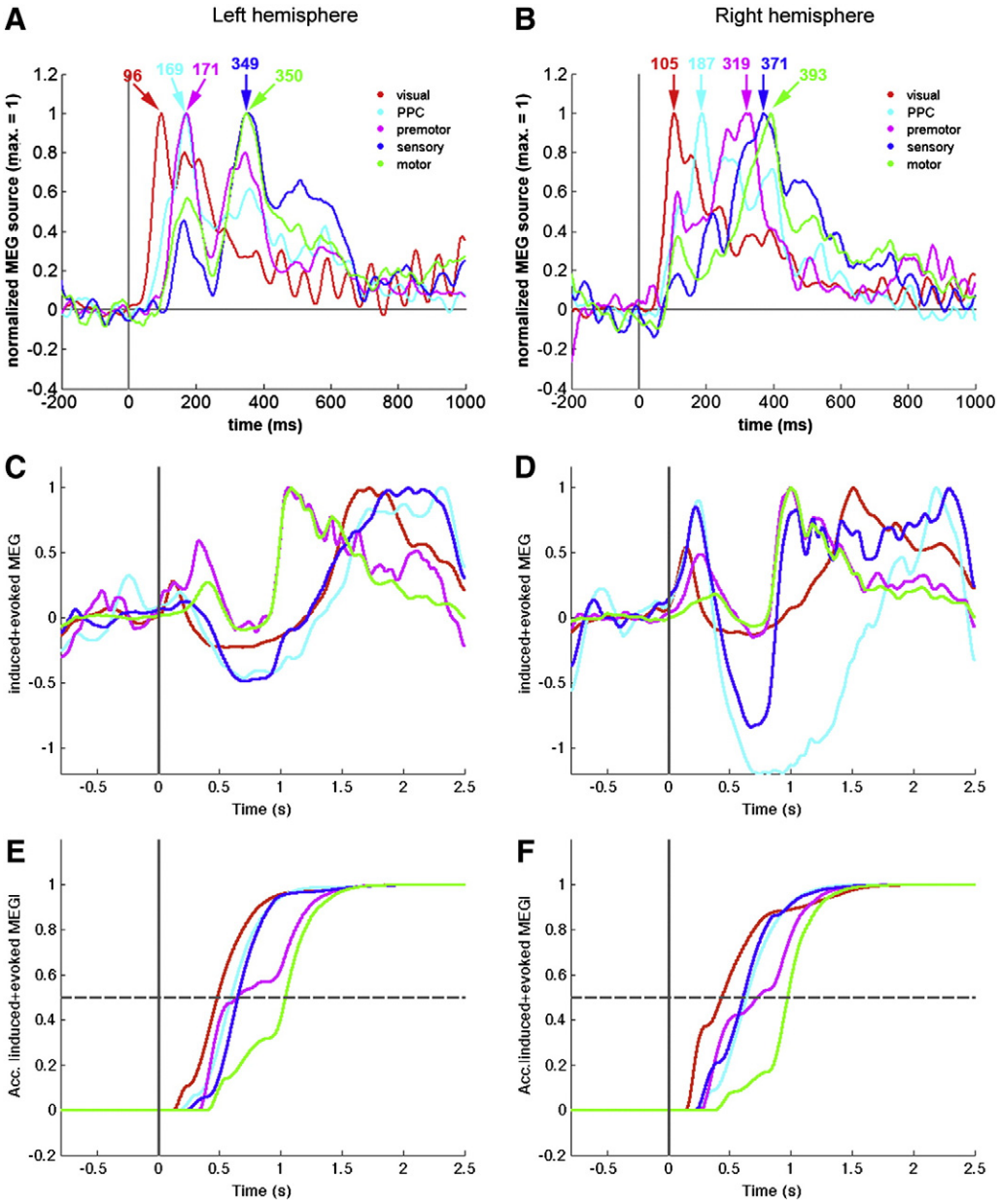

Fig. 5. MEG time courses. (A–B) Evoked responses. The waveforms are amplitude normalized (maximum for each response is 1). Visual cortex, PPC, premotor cortex, sensory cortex, and motor cortex reach the peak value sequentially in both the left and right hemispheres. The numbers in the figure indicate the time-to-peak. (C–D) Induced responses. Temporal spectral evolution (TSE) time courses show event-related synchronization (ERS), event-related de-synchronization (ERD), and rebound in both hemispheres. (E–F) Oscillatory timing index (OTI) results. For the induced responses, the window function $w(t)$ was generated to emphasize ERS/ERD that is best correlated with BOLD responses, and to exclude the rebound that is poorly correlated with BOLD responses; the peak latencies for each $w(t)$ were set at the TSE-ERS peak of the corresponding ROI. Then, to estimate the time course of neuronal power/energy consumption, the induced (TSE) responses were multiplied with the corresponding $w(t)$ for each ROI, and the cumulative integral of TSE $*$ $w(t)$ within the time window of 0–2 s was calculated. OTI values were picked at the time when this cumulative function reached 50% of its maximum.

between brain areas are caused by interregional variability in vasculature. However, the current study – the first to quantify this potential confound – found no statistically significant results to support this possibility. Therefore, if such vascular intrinsic effects exist, their influence (at least when averaging spatially within ROIs and across subjects) seems small compared with neuronally driven interregional delays. However, our results only demonstrated a double dissociation between the visual and motor cortices. Further studies are needed to ascertain similar effects across other brain areas.

Table 4
MEG induced response oscillatory timing index (*OTI*) latencies for all five ROIs (mean ± SEM).

OTI latency [ms]	Visual	PPC	Premotor	Somatosensory	Motor
Left hemisphere	480 ± 56	592 ± 68	640 ± 155	647 ± 62	1037 ± 214
Right hemisphere	432 ± 93	635 ± 58	726 ± 196	608 ± 37	971 ± 201

Inter-regional differences in neurovascular coupling have been documented extensively in literature. Some aspects of these differences have solid physiological basis, including post-capillary blood flow, penetrating venules and surface veins. This timing difference can be as large as 1–2 s. In fact, our results corroborated the finding about the spatial variability of the hemodynamic response (Figs. 2G and H). Therefore, although our results were based on 1) average within an ROI and 2) average across subjects, which allowed us to

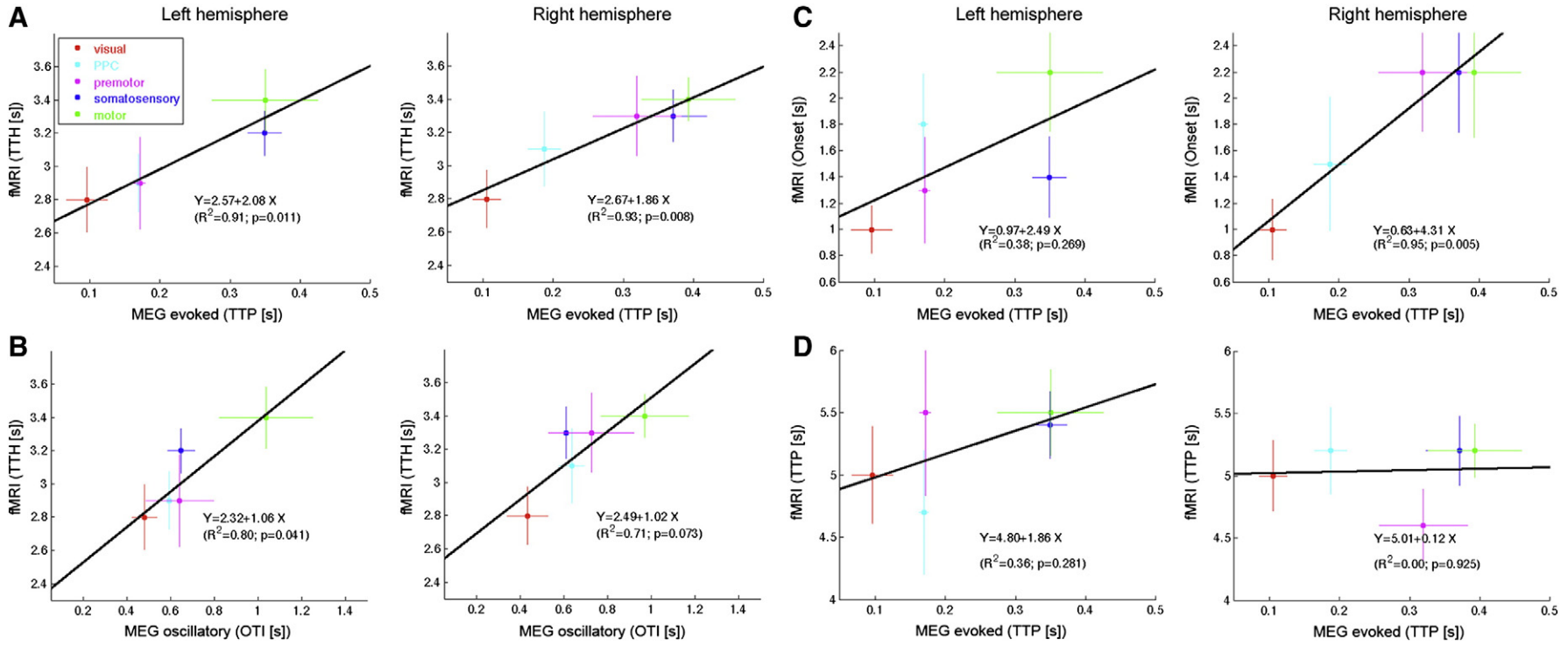

Fig. 6. Correlation between electrophysiological (MEG) and hemodynamic (BOLD) timing. A linear regression between source-specific MEG and BOLD (*TTH*) latencies was found separately in the left and right hemispheres using both the (A) evoked MEG response *TTP* values and (B) oscillatory MEG timing index *OTI* derived from induced responses. The slopes were about 2.3 for the evoked responses and 1.0 for the oscillatory analysis, indicating that the MEG induced responses may reflect BOLD interregional delays more faithfully than evoked responses. SEM error bars. A linear regression was also done between MEG and BOLD *Onset* latency (C) and *TTP* latency (D).

statistically reduce the contribution of vascular variation across different locations within one brain area and across different subjects, further studies are needed to affirm that neuronal delays can also be determined based on fMRI at the level of an individual subject.

It should be noted that we assumed that the temporal properties of the BOLD response for the motor/visual areas are constant between the main and control experiments. While this may not be the case due to anticipatory effects (Gibson et al., 2005), this effect was unlikely a significant confound due to the relatively simple nature of the task. Note also that in MEG/EEG literature, anticipation effects and attentional modulations, such as the so-called processing negativity (Näätänen, 1992), are observed as sustained amplitude modulations, instead of response latency modulations. Thus, we expect no significant anticipatory/attentional effects on our fMRI timing results, while further experiments validating this hypothesis will be certainly helpful.

The present study, to our knowledge, is the first one to compare interregional BOLD and MEG/EEG delays, showing that their correlation is approximately linear. This suggests that BOLD timing is fairly accurately driven by neuronal population-level postsynaptic potentials that MEG/EEG reflect (Okada et al., 1997). Therefore, BOLD fMRI can be a useful tool for studying neuronal activation sequences at realistically fast interregional delays. The delays started to be significant at 100 ms, at 200–300 ms about half of the delays were significant, and at ≥400 ms all delays were significant (Tables 1 and 2). Therefore, the effective temporal resolution for observing interregional BOLD delays in the present study was about 100–300 ms. It is presently unknown if this resolution can be further improved by technological advances (e.g., by sampling the BOLD responses even faster) or if physiological variability (e.g., across subjects and voxels) limits the achievable temporal accuracy. Our results suggested that the BOLD timing difference is comparable with the induced neural response but not the evoked neural response (Fig. 6). This finding on the close relationship between BOLD timing difference and induced neural response is consistent with previous observations (Muthukumaraswamy et al., 2009; Niessing et al., 2005). Our results indicated that the transduction of BOLD signal from neuronal activity is not a simple time-locked event but an integrative process.

Previously, it has been suggested that within-ROI delays to different types of stimuli could be resolved by fitting a canonical function and its temporal derivative on the BOLD data even at 100 ms temporal resolution, but that this method should not be applied to interregional delays due to unknown vascular confounds across regions (Friston et al., 1998). In the present study the interregional vascular confounds were characterized and found to be too small to bias the observed delays between ROIs. Moreover, the BOLD timings were derived directly from the HDRs at the native 100 ms temporal resolution without any *a priori* assumptions, therefore avoiding all potential biases inherent in using canonical basis functions or model fits that assume shapes and/or latencies of the BOLD responses.

Our results suggest that the different hemodynamic properties of the different ROIs are of lesser effect than the neuronal timing differences on the measured BOLD timing differences. Thus it is possible to use BOLD fMRI to measure fine timing differences (in the range of hundreds of milliseconds) in the brain, particularly in deep brain areas, where MEG and EEG are difficult to detect even though they have excellent millisecond temporal resolution. One potential application of this finding is on the effective connectivity analysis (Cabeza et al., 1997; Friston, 2007; Friston et al., 1997). Previously the causal interaction between brain areas estimated from BOLD fMRI signal has been questioned by the contribution of vascular effects. Now one might argue that, at least between the visual and somatomotor areas, the causal effects estimated by fast fMRI methods are neuronally driven.

The present study focused on the timing of group level BOLD responses, where the results were robust. However, we also found that at least 8 subjects were required to reach significance even for the coarsest timing difference between the visual and motor cortices. This finding is in accord with previous studies showing that at the individual level, interregional vascular confounds may overwhelm any neuronally related timing information. Future within-subjects studies are needed to illuminate the role of individual level interregional vascular differences. Such studies will also be useful for clarifying the relative contributions of (i) spatial averaging within ROIs within subjects and (ii) averaging across subjects in reducing the effect of interregional vascular differences.

The current results also show that InI allows whole-head BOLD imaging with high temporal resolution in realistically short experiments. Even traditional echo planar imaging (EPI) can achieve high temporal resolution with whole-head coverage through jittered stimulus timing (Friston, 2007; Rosen et al., 1998), but the duration of the experiment increases linearly with the ratio between TR and desired temporal resolution. For example, in order to achieve the same temporal resolution and whole-head spatial coverage as the present InI experiment, in which data collection took only 16 min, an EPI experiment with TR = 2 s would take 5 h.

InI uses a very short TR and consequently flip angle should be optimized in order to achieve the highest SNR. The T_1 value used for flip angle optimization in this study may not be exactly 1 s as measured in other studies (Wright et al., 2008). However, we consider 1 s to be a reasonable approximation, because ultimately it is the contrast-to-noise ratio, rather than the signal itself (related to the Ernst angle), that we attempt to optimize through flip angle selection. Corroborating this idea, a recent study (Gonzalez-Castillo et al., 2011) found that the BOLD percentage signal change was rather invariable across a wide range of flip angles. It therefore seems likely that any flip angle between 30° and 21° would have produced similar results.

More studies may be needed to understand why the delays appear to be longer in BOLD than in evoked MEG responses. This finding is consistent with previous studies showing that the interregional hemodynamic timing differences are longer than reaction times (Bellgowan et al., 2003; Henson et al., 2002). Potential explanations include low-pass filtering (Logothetis et al., 2001) and nonlinear (Devor et al., 2003) nature of neurovascular coupling, the exact way in which hemodynamic and neuronal latencies were measured, statistical power issues, possible cancelations of MEG sources with opposing directions (Ahlfors et al., 2010), and especially – because the interregional delays were much more similar between the induced MEG responses (*OTI*) and BOLD fMRI – the averaging process that removes out-of-phase MEG components from evoked responses. Nonetheless, the present results suggest new possibilities for what fMRI might tell us about the dynamic brain.

Acknowledgments

We are grateful for access to the MEG imaging resources at the Veteran General Hospital, Taipei, Taiwan, and the MRI resources at the National Yang-Ming University and National Taiwan University Hospital, Taipei, Taiwan. We also thank Academician Riitta Hari for comments, Chih-Che Chou and Yen-Hsiang Wang for technical support, and Nichole Eusemann for language editing. This work was supported by grants from the United States National Institutes of Health (NIH) (R01HD040712, R01NS037462, R01NS048279, P41RR014075, R01MH083744, R21DC010060, R21EB007298), National Center for Research Resources, National Science Council, Taiwan (NSC 101-2628-B-002-005-MY3, NSC 100-2325-B-002-046), National Health Research Institute, Taiwan (NHRI-EX102-10247EI), and Academy of Finland (127624 and the FiDiPro program).

Conflict of interest

All authors have no conflict of interest to disclose.

References

Aguirre, G.K., Zarahn, E., D'Esposito, M., 1998. The variability of human, BOLD hemodynamic responses. Neuroimage 8, 360–369.

Ahlfors, S.P., Simpson, G.V., Dale, A.M., Belliveau, J.W., Liu, A.K., Korvenoja, A., Virtanen, J., Huotilainen, M., Tootell, R.B., Aronen, H.J., Ilmoniemi, R.J., 1999. Spatiotemporal activity of a cortical network for processing visual motion revealed by MEG and fMRI. J. Neurophysiol. 82, 2545–2555.

Ahlfors, S.P., Han, J., Lin, F.H., Witzel, T., Belliveau, J.W., Hamalainen, M.S., Halgren, E., 2010. Cancellation of EEG and MEG signals generated by extended and distributed sources. Hum. Brain Mapp. 31, 140–149.

Ahonen, A., Hämäläinen, M., Kajola, M., Knuutila, J., Laine, P., Lounasmaa, O., Parkkonen, L., Simola, J., Tesche, C., 1993. 122-Channel SQUID instrument for investigating the magnetic signals from the human brain. Phys. Scr. T49, 198–205.

Babiloni, F., Babiloni, C., Carducci, F., Romani, G.L., Rossini, P.M., Angelone, L.M., Cincotti, F., 2003. Multimodal integration of high-resolution EEG and functional magnetic resonance imaging data: a simulation study. Neuroimage 19, 1–15.

Bellgowan, P.S., Saad, Z.S., Bandettini, P.A., 2003. Understanding neural system dynamics through task modulation and measurement of functional MRI amplitude, latency, and width. Proc. Natl. Acad. Sci. U. S. A. 100, 1415–1419.

Belliveau, J., Kennedy, D., McKinstry, R., Buchbinder, B., Weisskoff, R., Cohen, M., Vevea, J., Brady, T., Rosen, B., 1991. Functional mapping of the human visual cortex by magnetic resonance imaging. Science 254, 716–719.

Brainard, D.H., 1997. The psychophysics toolbox. Spat. Vis. 10, 433–436.

Brookes, M.J., Gibson, A.M., Hall, S.D., Furlong, P.L., Barnes, G.R., Hillebrand, A., Singh, K.D., Holliday, I.E., Francis, S.T., Morris, P.G., 2005. GLM-beamformer method demonstrates stationary field, alpha ERD and gamma ERS co-localisation with fMRI BOLD response in visual cortex. Neuroimage 26, 302–308.

Burock, M., Dale, A., 2000. Estimation and detection of event-related fMRI signals with temporally correlated noise: a statistically efficient and unbiased approach. Hum. Brain Mapp. 11, 249–260.

Cabeza, R., McIntosh, A.R., Tulving, E., Nyberg, L., Grady, C.L., 1997. Age-related differences in effective neural connectivity during encoding and recall. Neuroreport 8, 3479–3483.

Chernick, M., 2007. Bootstrap Methods: A Guide for Practitioners and Researchers, 2nd ed. Wiley, New York.

Cohen, D., Schlapfer, U., Ahlfors, S., Hamalainen, M., Halgren, E., 2002. New six-layer magnetically-shielded room for MEG. In: Nowak, H., Haueisen, J., Giessler, F., Huonker, R. (Eds.), 13th International Conference on Biomagnetism. VDE Verlag, Jena, Germany, pp. 919–921.

Dale, A., Buckner, R., 1997. Selective averaging of individual trials using fMRI. Hum. Brain Mapp. 5, 329–340.

Dale, A.M., Fischl, B., Sereno, M.I., 1999. Cortical surface-based analysis. I. Segmentation and surface reconstruction. Neuroimage 9, 179–194.

Dale, A., Liu, A., Fischl, B., Buckner, R., Belliveau, J., Lewine, J., Halgren, E., 2000. Dynamic statistical parametric mapping: combining fMRI and MEG for high-resolution imaging of cortical activity. Neuron 26, 55–67.

Descamps, B., Vandemaele, P., Reyngoudt, H., Deblaere, K., Leybaert, L., Paemeleire, K., Achten, E., 2012. Quantifying hemodynamic refractory bold effects in normal subjects at the single-subject level using an inverse logit fitting procedure. J. Magn. Reson. Imaging 35, 723–730.

Devor, A., Dunn, A.K., Andermann, M.L., Ulbert, I., Boas, D.A., Dale, A.M., 2003. Coupling of total hemoglobin concentration, oxygenation, and neural activity in rat somatosensory cortex. Neuron 39, 353–359.

Fischl, B., Sereno, M., Dale, A., 1999a. Cortical surface-based analysis. II: inflation, flattening, and a surface-based coordinate system. Neuroimage 9, 195–207.

Fischl, B., Sereno, M., Tootell, R., Dale, A., 1999b. High-resolution inter-subject averaging and a coordinate system for the cortical surface. Hum. Brain Mapp. 8, 272–284.

Fischl, B., Liu, A., Dale, A.M., 2001. Automated manifold surgery: constructing geometrically accurate and topologically correct models of the human cerebral cortex. IEEE Trans. Med. Imaging 20, 70–80.

Formaggio, E., Storti, S.F., Avesani, M., Cerini, R., Milanese, F., Gasparini, A., Acler, M., Pozzi Mucelli, R., Fiaschi, A., Manganotti, P., 2008. EEG and FMRI coregistration to investigate the cortical oscillatory activities during finger movement. Brain Topogr. 21, 100–111.

Formisano, E., Linden, D.E., Di Salle, F., Trojano, L., Esposito, F., Sack, A.T., Grossi, D., Zanella, F.E., Goebel, R., 2002. Tracking the mind's image in the brain I: time-resolved fMRI during visuospatial mental imagery. Neuron 35, 185–194.

Friston, K.J., 2007. Statistical Parametric Mapping: The Analysis of Functional Brain Images, 1st ed. Academic Press, Amsterdam; Boston.

Friston, K.J., Buechel, C., Fink, G.R., Morris, J., Rolls, E., Dolan, R.J., 1997. Psychophysiological and modulatory interactions in neuroimaging. Neuroimage 6, 218–229.

Friston, K.J., Fletcher, P., Josephs, O., Holmes, A., Rugg, M.D., Turner, R., 1998. Event-related fMRI: characterizing differential responses. Neuroimage 7, 30–40.

George, J.S., Aine, C.J., Mosher, J.C., Schmidt, D.M., Ranken, D.M., Schlitt, H.A., Wood, C.C., Lewine, J.D., Sanders, J.A., Belliveau, J.W., 1995. Mapping function in the human brain with magnetoencephalography, anatomical magnetic resonance imaging, and functional magnetic resonance imaging. J. Clin. Neurophysiol. 12, 406–431.

Gibson, A.M., Brookes, M.J., Kim, S.S., Francis, S.T., Morris, P.G., 2005. A new quantitative analysis of significant timing differences between externally cued and self-initiated motor tasks in an fMRI study. Solid State Nucl. Magn. Reson. 28, 258–265.

Gonzalez-Castillo, J., Roopchansingh, V., Bandettini, P.A., Bodurka, J., 2011. Physiological noise effects on the flip angle selection in BOLD fMRI. Neuroimage 54, 2764–2778.

Hämäläinen, M., Sarvas, J., 1989. Realistic conductivity geometry model of the human head for interpretation of neuromagnetic data. IEEE Trans. Biomed. Eng. 36, 165–171.

Hämäläinen, M., Hari, R., Ilmoniemi, R., Knuutila, J., Lounasmaa, O., 1993. Magnetoencephalography—theory, instrumentation, and application to noninvasive studies of the working human brain. Rev. Mod. Phys. 65, 413–497.

Hari, R., Salmelin, R., Makela, J.P., Salenius, S., Helle, M., 1997. Magnetoencephalographic cortical rhythms. Int. J. Psychophysiol. 26, 51–62.

Henson, R.N., Price, C.J., Rugg, M.D., Turner, R., Friston, K.J., 2002. Detecting latency differences in event-related BOLD responses: application to words versus nonwords and initial versus repeated face presentations. Neuroimage 15, 83–97.

Huettel, S., McCarthy, G., 2000. Evidence for a refractory period in the hemodynamic response to visual stimuli as measured by MRI. Neuroimage 11, 547–553.

Kim, S.G., Ogawa, S., 2002. Insights into new techniques for high resolution functional MRI. Curr. Opin. Neurobiol. 12, 607–615.

Kwong, K.K., Belliveau, J.W., Chesler, D.A., Goldberg, I.E., Weisskoff, R.M., Poncelet, B.P., Kennedy, D.N., Hoppel, B.E., Cohen, M.S., Turner, R., Cheng, H., Brady, T.J., Rosen, B.R., 1992. Dynamic magnetic resonance imaging of human brain activity during primary sensory stimulation. Proc. Natl. Acad. Sci. U. S. A. 89, 5675–5679.

Lachaux, J.P., Rodriguez, E., Martinerie, J., Varela, F.J., 1999. Measuring phase synchrony in brain signals. Hum. Brain Mapp. 8, 194–208.

Lee, A.T., Glover, G.H., Meyer, C.H., 1995. Discrimination of large venous vessels in time-course spiral blood-oxygen-level-dependent magnetic-resonance functional neuroimaging. Magn. Reson. Med. 33, 745–754.

Lin, F.H., Witzel, T., Hamalainen, M.S., Dale, A.M., Belliveau, J.W., Stufflebeam, S.M., 2004. Spectral spatiotemporal imaging of cortical oscillations and interactions in the human brain. Neuroimage 23, 582–595.

Lin, F.H., Witzel, T., Mandeville, J.B., Polimeni, J.R., Zeffiro, T.A., Greve, D.N., Wiggins, G., Wald, L.L., Belliveau, J.W., 2008. Event-related single-shot volumetric functional magnetic resonance inverse imaging of visual processing. Neuroimage 42, 230–247.

Lin, F.H., Witzel, T., Chang, W.T., Wen-Kai Tsai, K., Wang, Y.H., Kuo, W.J., Belliveau, J.W., 2010. K-space reconstruction of magnetic resonance inverse imaging (K-InI) of human visuomotor systems. Neuroimage 49, 3086–3098.

Liu, A.K., Belliveau, J.W., Dale, A.M., 1998. Spatiotemporal imaging of human brain activity using functional MRI constrained magnetoencephalography data: Monte Carlo simulations. Proc. Natl. Acad. Sci. U. S. A. 95, 8945–8950.

Liu, A., Dale, A., Belliveau, J., 2002. Monte Carlo simulation studies of EEG and MEG localization accuracy. Hum. Brain Mapp. 16, 47–62.

Liu, H.L., Feng, C.M., Li, J., Su, F.C., Li, N., Glahn, D., Gao, J.H., 2005. Disparity of activation onset in sensory cortex from simultaneous auditory and visual stimulation: differences between perfusion and blood oxygenation level-dependent functional magnetic resonance imaging. J. Magn. Reson. Imaging 21, 111–117.

Logothetis, N., Pauls, J., Augath, M., Trinath, T., Oeltermann, A., 2001. Neurophysiological investigation of the basis of the fMRI signal. Nature 412, 150–157.

Menon, R.S., Kim, S.G., 1999. Spatial and temporal limits in cognitive neuroimaging with fMRI. Trends Cogn. Sci. 3, 207–216.

Menon, R.S., Luknowsky, D.C., Gati, J.S., 1998. Mental chronometry using latency-resolved functional MRI. Proc. Natl. Acad. Sci. U. S. A. 95, 10902–10907.

Miezin, F.M., Maccotta, L., Ollinger, J.M., Petersen, S.E., Buckner, R.L., 2000. Characterizing the hemodynamic response: effects of presentation rate, sampling procedure, and the possibility of ordering brain activity based on relative timing. Neuroimage 11, 735–759.

Muthukumaraswamy, S.D., Singh, K.D., 2008. Spatiotemporal frequency tuning of BOLD and gamma band MEG responses compared in primary visual cortex. Neuroimage 40, 1552–1560.

Muthukumaraswamy, S.D., Edden, R.A., Jones, D.K., Swettenham, J.B., Singh, K.D., 2009. Resting GABA concentration predicts peak gamma frequency and fMRI amplitude in response to visual stimulation in humans. Proc. Natl. Acad. Sci. U. S. A. 106, 8356–8361.

Näätänen, R., 1992. Attention and Brain Function. L. Erlbaum, Hillsdale, N.J.

Niessing, J., Ebisch, B., Schmidt, K.E., Niessing, M., Singer, W., Galuske, R.A., 2005. Hemodynamic signals correlate tightly with synchronized gamma oscillations. Science 309, 948–951.

Ogawa, S., Tank, D.W., Menon, R., Ellermann, J.M., Kim, S.-G., Merkle, H., Ugurbil, K., 1992. Intrinsic signal changes accompanying sensory stimulation: functional brain mapping with magnetic resonance imaging. Proc. Natl. Acad. Sci. U. S. A. 89, 5951–5955.

Ogawa, S., Lee, T.M., Stepnoski, R., Chen, W., Zhu, X.H., Ugurbil, K., 2000. An approach to probe some neural systems interaction by functional MRI at neural time scale down to milliseconds. Proc. Natl. Acad. Sci. U. S. A. 97, 11026–11031.

Okada, Y.C., Wu, J., Kyuhou, S., 1997. Genesis of MEG signals in a mammalian CNS structure. Electroencephalogr. Clin. Neurophysiol. 103, 474–485.

Pelli, D.G., 1997. The VideoToolbox software for visual psychophysics: transforming numbers into movies. Spat. Vis. 10, 437–442.

Richter, W., Ugurbil, K., Georgopoulos, A., Kim, S.G., 1997. Time-resolved fMRI of mental rotation. Neuroreport 8, 3697–3702.

Richter, W., Somorjai, R., Summers, R., Jarmasz, M., Menon, R.S., Gati, J.S., Georgopoulos, A.P., Tegeler, C., Ugurbil, K., Kim, S.G., 2000. Motor area activity during mental rotation studied by time-resolved single-trial fMRI. J. Cogn. Neurosci. 12, 310–320.

Rosa, M.J., Daunizeau, J., Friston, K.J., 2010. EEG-fMRI integration: a critical review of biophysical modeling and data analysis approaches. J. Integr. Neurosci. 9, 453–476.

Rosen, B.R., Buckner, R.L., Dale, A.M., 1998. Event-related functional MRI: past, present, and future. Proc. Natl. Acad. Sci. U. S. A. 95, 773–780.

Salmelin, R., Hari, R., 1994. Spatiotemporal characteristics of sensorimotor neuromagnetic rhythms related to thumb movement. Neuroscience 60, 537–550.
Sharon, D., Hamalainen, M.S., Tootell, R.B., Halgren, E., Belliveau, J.W., 2007. The advantage of combining MEG and EEG: comparison to fMRI in focally stimulated visual cortex. Neuroimage 36, 1225–1235.
Sigman, M., Jobert, A., Lebihan, D., Dehaene, S., 2007. Parsing a sequence of brain activations at psychological times using fMRI. Neuroimage 35, 655–668.
Vanni, S., Warnking, J., Dojat, M., Delon-Martin, C., Bullier, J., Segebarth, C., 2004. Sequence of pattern onset responses in the human visual areas: an fMRI constrained VEP source analysis. Neuroimage 21, 801–817.
Waugh, C.E., Wager, T.D., Fredrickson, B.L., Noll, D.C., Taylor, S.F., 2008. The neural correlates of trait resilience when anticipating and recovering from threat. Soc. Cogn. Affect. Neurosci. 3, 322–332.
Weilke, F., Spiegel, S., Boecker, H., von Einsiedel, H.G., Conrad, B., Schwaiger, M., Erhard, P., 2001. Time-resolved fMRI of activation patterns in M1 and SMA during complex voluntary movement. J. Neurophysiol. 85, 1858–1863.
Wright, P.J., Mougin, O.E., Totman, J.J., Peters, A.M., Brookes, M.J., Coxon, R., Morris, P.E., Clemence, M., Francis, S.T., Bowtell, R.W., Gowland, P.A., 2008. Water proton T1 measurements in brain tissue at 7, 3, and 1.5 T using IR-EPI, IR-TSE, and MPRAGE: results and optimization. MAGMA 21, 121–130.